



Nano-SiO₂@PMMA-doped composite polymer PVDF-HFP/PMMA/PEO electrolyte for lithium metal batteries

Jian Li^{1,2} · Rong Hu¹ · Hongming Zhou^{1,2} · Shengdong Tao¹ · Ya Wang¹

Received: 5 June 2019 / Accepted: 22 December 2019 / Published online: 14 January 2020
© Springer Science+Business Media, LLC, part of Springer Nature 2020

Abstract

Polymer electrolytes have attracted widespread attention owing to their low cost and excellent processability. However, polymer electrolytes have yet been widely applied in commercial batteries due to their own drawbacks, such as weak mechanical properties and lower ionic conductivity. In this paper, poly(vinylidene fluoride-co-hexafluoropropylene) (PVDF-HFP) was blended with polyethylene oxide (PEO) and polymethyl methacrylate (PMMA) to build a novel polymer matrix, and SiO₂@PMMA was doped into blended polymer matrix to form a composite polymer electrolyte named CPE-(SiO₂@PMMA). The CPE-(SiO₂@PMMA) performs superior electrochemical performance, such as a favorable electrochemical stability window (4.7 V vs Li/Li⁺), decent ionic conductivity (8.54×10^{-5} S cm⁻¹ at 60 °C), and excellent interface stability. The lithium metal battery LiNi_{0.8}Co_{0.1}Mn_{0.1}O₂/CPE/Li was fabricated to build a high specific energy system, which performs excellent cycling and C-rate performance compared to others polymer electrolytes. Capacity retention of LiNi_{0.8}Co_{0.1}Mn_{0.1}O₂/Li cell with CPE-(SiO₂@PMMA) achieves 81.6% after 100 cycles, while CPE was broken with 100 cycles unfinished. All of the above favorable properties proved that PVDF-HFP/PMMA/PEO polymer matrix with SiO₂@PMMA doped is a promising electrolyte candidate for flexible lithium metal batteries.

1 Introduction

Lithium metal batteries owing to their inherent advantages of high energy density are expected to be applied in many situations; however, the growth of lithium dendrites seriously hinders the practical application of lithium metal batteries [1–3]. In addition, the flammable alkyl carbonate electrolyte solvent in the liquid electrolyte of lithium ion batteries still has safety hazards [4, 5]. We urgently need a series of substantial improvements to address these critical issues; an effective way to improve security is to use a solid-state battery of non-flammable solid ionic conductor design. Therefore, solid electrolytes have attracted the attention of researchers around the world.

Solid polymer electrolytes turn out to be an effective way to address the problem mentioned above; they exhibit many advantages, such as non-toxicity, significant processing

advantages, non-flammability, and the uniform deposition of lithium [4–8]. However, mediocre ionic conductivity at ambient temperature and weak mechanical properties greatly limit their actualization application [4, 6]. Multiple polymers have been investigated as solid polymer electrolytes matrix, such as polyethylene oxide (PEO), polymethyl methacrylate (PMMA), poly(vinylidene fluoride-co-hexafluoropropylene) (PVDF-HFP), poly(acrylonitrile) (PAN), and polymeric siloxanes (PSs) [5, 7–15]. Among these, PEO has advantages in dimensional flexibility, high lithium salt solubility, excellent stability in contact with Li metal, and excellent mechanical properties. However, PEO is easily crystallized at low temperatures and the ionic conductivity is low at room temperature [4, 5, 7–9]. PMMA is a typical amorphous polymer, which has favorable dimensional stability, flexibility, and stable contact with lithium, but its poor mechanical properties hinder its practical application [10–15]. PVDF-HFP has high dielectric and good electrochemical stability; in addition, crystallinity has been reduced due to HFP component. But it is difficult to form a suitable solid-state polymer electrolytes with high ionic conductivity and the cost is still high [15, 16]. Therefore, a single-component polymer matrix cannot meet the requirements for practical application. Polymer blending [16–19], co-polymerization

✉ Hongming Zhou
zhouhongming@csu.edu.cn

¹ School of Materials Science and Engineering, Central South University, Changsha 410083, Hunan, China

² Hunan Zhengyuan Institute for Energy Storage Materials and Devices, Changsha 410083, Hunan, China

[19, 20], and crosslinking [21, 22] are effective methods to enhance the performance of the polymer matrix. Polymer blending eliminates the shortcomings of the performance of the single polymer component, maintains their respective advantages, and then obtains a polymer material with excellent comprehensive properties. Tsao [16] found that the gel polymer electrolyte based on the blend polymer polydimethylsiloxane (PDMS)/ poly(acrylonitrile) (PAN)/PEO exhibited high active Li^+ transport number and excellent ionic conductivity. Idris [17] reported that amorphous polymer PMMA blended with PVDF promoted the migration of lithium ion which increased ionic conductivity effectively, but led to the weak mechanical performance.

It is also acknowledged that the moderate addition of nanoscale inorganic fillers (SiO_2 [23–26], TiO_2 [27, 28], and Al_2O_3 [29]) can ameliorate the performances of polymer electrolytes, including the mechanical strength, thermal stability, and ionic conductivity. Among these, SiO_2 particles have been proven to efficiently improve electrochemical stability of Li/electrolyte interface [23–26]. However, due to the low Zeta potential and high surface energy of the nanoinorganic particles, the particles are easily agglomerated. These agglomerated nanoparticles hardly exert the characteristics possessed by the nanomaterials themselves, which will inevitably affect the ion conductivity of the composite electrolyte and electrochemical performances of the polymer battery [30]. Hence, how to disperse the nanoscale inorganic oxides in an appropriate content in the polymer matrix is a key issue. Nanoparticle coating is one of the effective ways to improve the dispersibility in polymer matrix [31–34]. Cao [32] prepared a nanocrystalline TiO_2 -PMMA hybrid material hybridized with TiO_2 sol-PMMA precursor by in-situ heating. The nanocrystalline mixture can be dispersed in the PVDF-HFP matrix and enhance the properties of the polymer matrix PVDF-HFP in terms of pore distribution, electrolyte absorption, and ionic conductivity. Zuo [33] grafted the amino group on the surface of the SiO_2 nanoparticles, which improves the dispersion of the SiO_2 nanoparticles in the polymer matrix, provides a good channel for the lithium ions, and improves the thermal stability of the separator.

In this paper, we describe a successful fabrication of organic–inorganic hybrid particles SiO_2 @PMMA by in-situ polymerization, and doped SiO_2 @PMMA into a blended matrix (PVDF-HFP/PEO/PMMA) to form a novel composite polymer electrolyte. The coating layer of inorganic nanoparticles has the same composition with the blended polymer matrix which is PMMA, improving interface compatibility and dispersion of nanoparticles in polymer matrix effectively. A composite polymer electrolyte embedded with SiO_2 @PMMA nanoparticles showed great thermal stability, a wide electrochemical window, good interfacial compatibility with lithium metal, and a high ion conductivity. Furthermore, a solid-state $\text{LiNi}_{0.8}\text{Co}_{0.1}\text{Mn}_{0.1}\text{O}_2/\text{Li}$ half-cell

was constructed, which delivered excellent cycling and rate performance compared with other electrolytes.

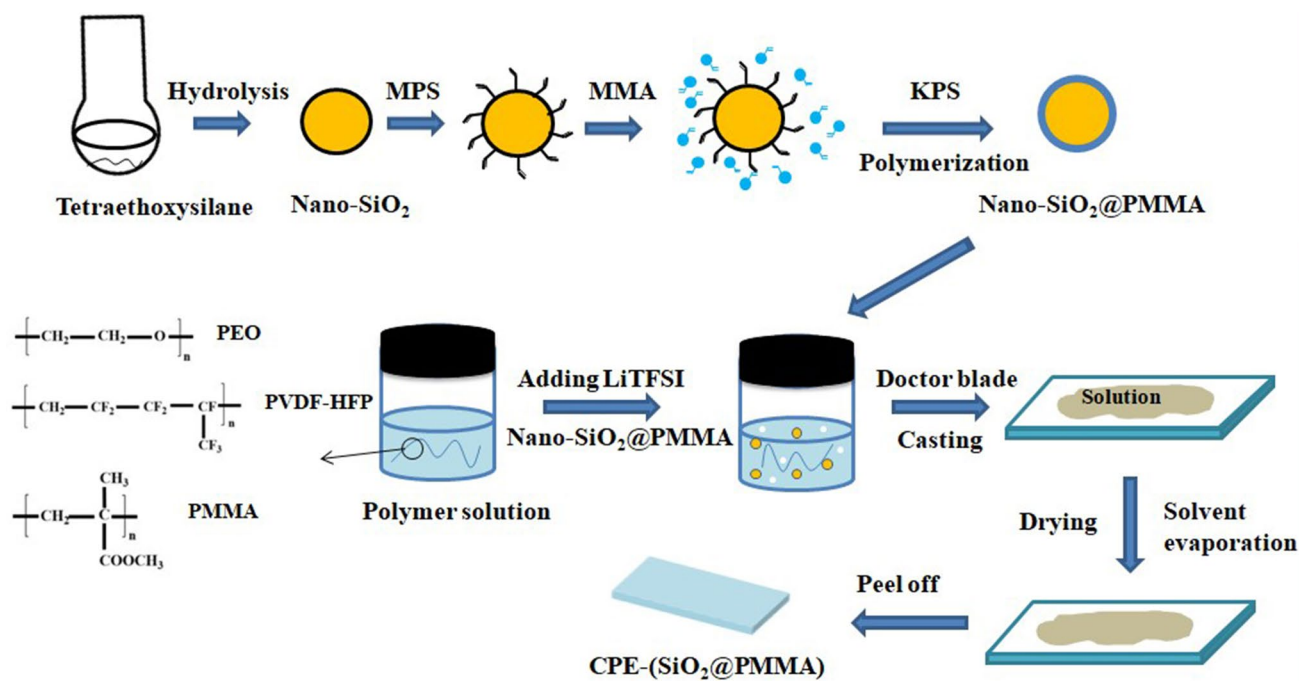
2 Experimental section

2.1 Synthesis of the hybrid particles SiO_2 @PMMA

Tetraethyl orthosilicate (TEOS, 98%) and ammonium hydroxide (28%) were analytical grade and used as received. Nano- SiO_2 particles were prepared by modified Stober method according to the literature [35]. The nano- SiO_2 particles was modified with 3-(trimethoxysilyl) propyl methacrylate (MPS, 98%) by dispersing silica nanoparticles and MPS into 200-proof ethanol with the aid of stirring at room temperature for 48 h. The suspension was then purified by centrifugal washing using ethanol. Seeded emulsion polymerization was used to synthesize SiO_2 @PMMA nanoparticles [36, 37]. In a typical synthesis, MPS-modified nano- SiO_2 particles, methyl methacrylate (MMA), sodium dodecyl sulfate (SDS, 99%), water, and 200-proof ethanol were mixed in a three-necked round-bottomed flask. After degassing with nitrogen in 50 °C to pre-emulsified for 30 min, the mixture was heated to 80 °C, and then a potassium persulfate (KPS) solution was injected into solution to initiate the polymerization. This reaction was maintained at 80 °C for 10 h. Centrifuged and washed particles repeatedly with absolute ethanol and acetone to remove unreacted MMA, and vacuum dried particles at 60 °C for 48 h.

2.2 Preparation of composite polymer electrolyte

Solvent casting technique was used to prepare the composite electrolyte as shown in Scheme 1. PVDF-HFP ($M_w = 4 \times 10^5$, Sigma), PEO ($M_w = 1 \times 10^6$, Aladdin), and PMMA ($M_w = 35,000$, Aladdin) were vacuum dried at 60 °C for 12 h before use. PVDF-HFP, PEO, and PMMA in an optimized mole ratio of 3:1:1 were dissolved in DMF–acetonitrile (3:1 (v/v)) mixed solution by magnetic stirring overnight at room temperature. Nano- SiO_2 @PMMA particles (4 wt% of polymer matrix) were well dispersed in DMF by ultrasonication for 20 min. Then, nano- SiO_2 @PMMA colloid and 2 wt% LiTFSI were added into the above solution, and the solution was stirred for 5 h to get a homogeneous solution. After sufficiently stirring, the slurry was cast in a Teflon disk. The solvent was slowly volatilized by passing nitrogen gas at room temperature for 24 h, and the polymer film was vacuum dried at 60–80 °C for 48 h, named CPE- (SiO_2 @PMMA). The mechanical properties of the membrane are stable and the polymer film obtained had a thickness of about 40–60 μm , and the surface of the membrane was smooth and non-microporous. Meanwhile, polymer electrolytes with nano- SiO_2 doped and without filler doped



Scheme 1 Synthesis of SiO₂@PMMA and the inorganic/organic composite polymer network

were also prepared, named CPE-SiO₂ and CPE. The dried CPE was stored in an argon-filled glove box before using.

2.3 Assembly of cells

The LiNi_{0.8}Co_{0.1}Mn_{0.1}O₂/Li half cells were employed to test electrochemical performance. The cathode was prepared by 80 wt% LiNi_{0.8}Co_{0.1}Mn_{0.1}O₂ active material, 10 wt% Polyvinylidene Fluoride (PVDF), and 10 wt% carbon black in *N*-methyl-pyrrolidone (NMP) as solvent, and the solution was stirred sufficiently in order to form a homogeneous slurry. The slurry was then cast on Al foil and dried at 80 °C for 12 h under vacuum. A cell was assembled in a 2032 coin cell by sandwiching a composite electrolyte between a LiNi_{0.8}Co_{0.1}Mn_{0.1}O₂ cathode and a lithium metal anode in the argon-filled glove box. During assembly, 50 μl of electrolyte was added to optimize the interface between the positive electrode and the electrolyte.

2.4 Materials characterization

The functional group, chemical bond of SiO₂ nanoparticles (SiO₂, SiO₂@PMMA) and different composite electrolyte membranes were recorded by Fourier transform infrared (FTIR) in the wavenumber between 4000 and 400 cm⁻¹. X-ray photoelectron Spectroscopy (XPS, ESCALab250Xi, ThermoFisher-VG Scientific) was used to further confirm the composition of the as-prepared materials. The morphologies of SiO₂ nanoparticles (SiO₂, SiO₂@PMMA) and different

composite electrolyte membranes were examined by a field-emission scanning electron microscope (SEM) and transmission electron microscopy (TEM). The content of PMMA in the SiO₂@PMMA nanospheres and the thermal stability of the composite membrane were performed by Thermogravimetric (TG) from 30 to 650 °C under a N₂ atmosphere using a heating rate of 10 °C min⁻¹. The crystallinity of the polymer was characterized by X-ray diffraction (XRD) using Cu Kα radiation. The diffraction angle (2θ) was set between 10° and 80° with a scan speed of 10° min⁻¹.

2.5 Electrochemical measurement

The ionic conductivity of composite electrolyte was measured by electrochemical impedance spectroscopy (EIS) using a blocking symmetric steel/CPE/steel cell from 1 MHz to 0.01 Hz at temperature of 20–80 °C with an amplitude of 10 mV. The ionic conductivity (σ) from the bulk resistance (R_b) can be calculated by equation:

$$\sigma = L / (R_b \times S),$$

where R_b and L are the electrolyte resistance and the thickness of the composite electrolyte, and S is the area contact between composite electrolyte and electrode.

The linear sweep voltammetry (LSV) from 3.0 to 6.0 V with a scanning rate of 0.5 mV s⁻¹ was performed using SS/electrolyte/Li cells. EIS was used to evaluate the interfacial compatibility with the lithium electrode by using

Li/composite electrolyte/Li cell in different times. The frequency range is 100 kHz to 1 Hz and EIS amplitude is 5 mV. All cells were assembled in a argon-filled glove box. The charge and discharge cycling testing and C-rate capability were performed by a battery tester (CT 4008, Neware, China), and the voltage range is from 2.8 to 4.3 V, respectively (1 C = 207 mAh g⁻¹). All the cells were tested at 0.1, 0.2, 0.5, 1, 2, 5 C for 10 cycles and finally return to 0.2 C at 60 °C to test C-rate capability.

3 Results and discussion

3.1 Characterization of SiO₂@PMMA nanoparticles

FTIR was used to survey the molecular composition of the SiO₂ nanoparticles before and after the modification. As is shown in Fig. 1a, significant Si–O–Si asymmetric and symmetric stretching vibration absorption peaks can be observed at 1100 and 802 cm⁻¹ [31]. The peak at 3437 cm⁻¹ corresponds to the –OH stretching vibration peak [36]. After MMA monomers polymerize onto the surface of the SiO₂ nanoparticles as presented in Fig. 1b, a new peak appears at 1731 cm⁻¹ corresponding to C=O bond from PMMA, and the peaks between 750 and 1300 cm⁻¹ become broad owing to the –C–O–C– bonds stretching mode from PMMA

[31, 36]. Meanwhile, the –OH stretching vibration peak at 3437 cm⁻¹ still can be observed, indicating that surface of SiO₂@PMMA still exists –OH groups [38]. TG was employed to determine the weight ratio of inorganic/organic hybrid nanocomposites. A rapid weight loss around 300–400 °C can be found in Fig. 1b, which is primarily attributed to the dehydrogenation of PMMA [31, 32]. The inorganic SiO₂ core remains after the decomposition of PMMA, indicating a weight ratio of about 60% for SiO₂@PMMA nanoparticles. Figure 1c, d reveals the XPS spectra of SiO₂ and SiO₂@PMMA nanoparticles. Figure 1c proves that SiO₂ consists of Si and O elements, while it is obvious that the Si, C, and O elements appear in the full element scan of SiO₂@PMMA. As shown in Fig. 1d, three obvious peaks of C 1s at 284.8 eV, 286.5 eV, and 288.9 eV were assigned to C–C, C–O, and O–C=O bonds, which correspond to the three structural carbons in the polymer PMMA [39]. Furthermore, the peak of Si 2p appears at 103.7 eV, which further proves that the Si element in SiO₂@PMMA exists mainly in the form of SiO₂.

Figure 2a shows the morphologies of SiO₂ nanoparticles prepared by Stober method. It can be found that SiO₂ nanoparticles are spherical with uniform particle size, which is consistent with the previous literature [36, 37]. The average particle diameter of SiO₂ nanoparticles is about 120 nm. After grafting the MMA monomers onto the surface of

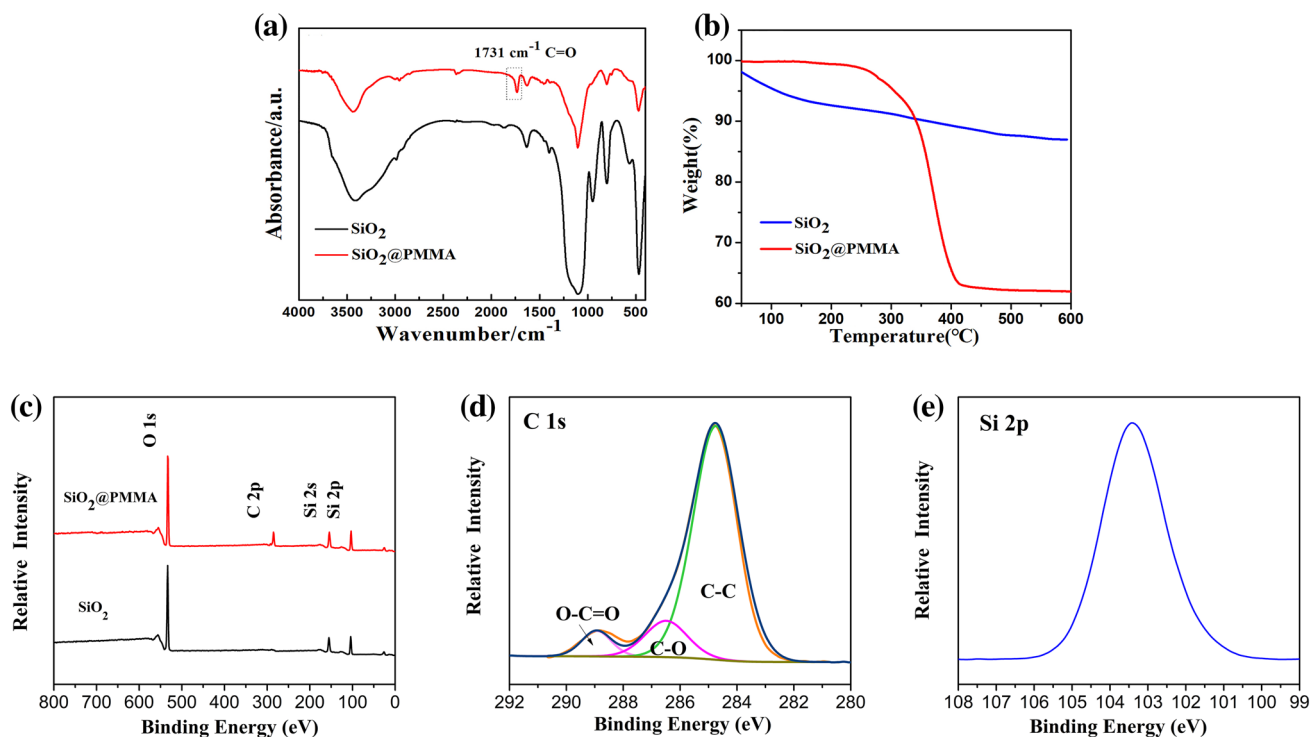


Fig. 1 **a** FTIR spectra of SiO₂ nanoparticles and SiO₂@PMMA nanoparticles. **b** TG curves of SiO₂ nanoparticles and SiO₂@PMMA nanoparticles. **c** XPS survey spectrum of SiO₂ nanoparticles and SiO₂@PMMA nanoparticles. **d** C 1s, **e** Si 2p of SiO₂@PMMA nanoparticles

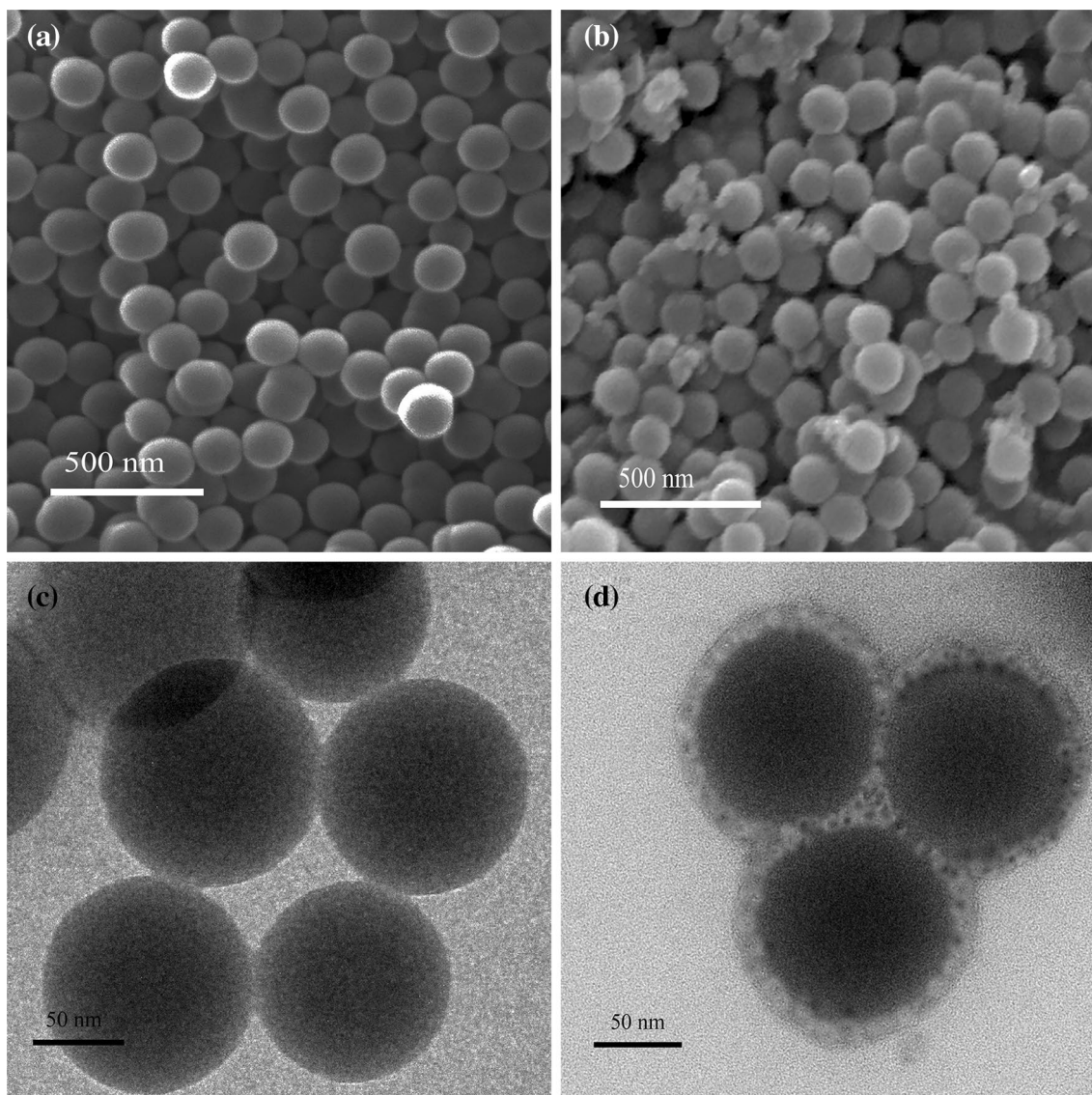


Fig. 2 SEM images of **a** SiO₂, **b** SiO₂@PMMA. TEM images of **c** SiO₂, **d** SiO₂@PMMA

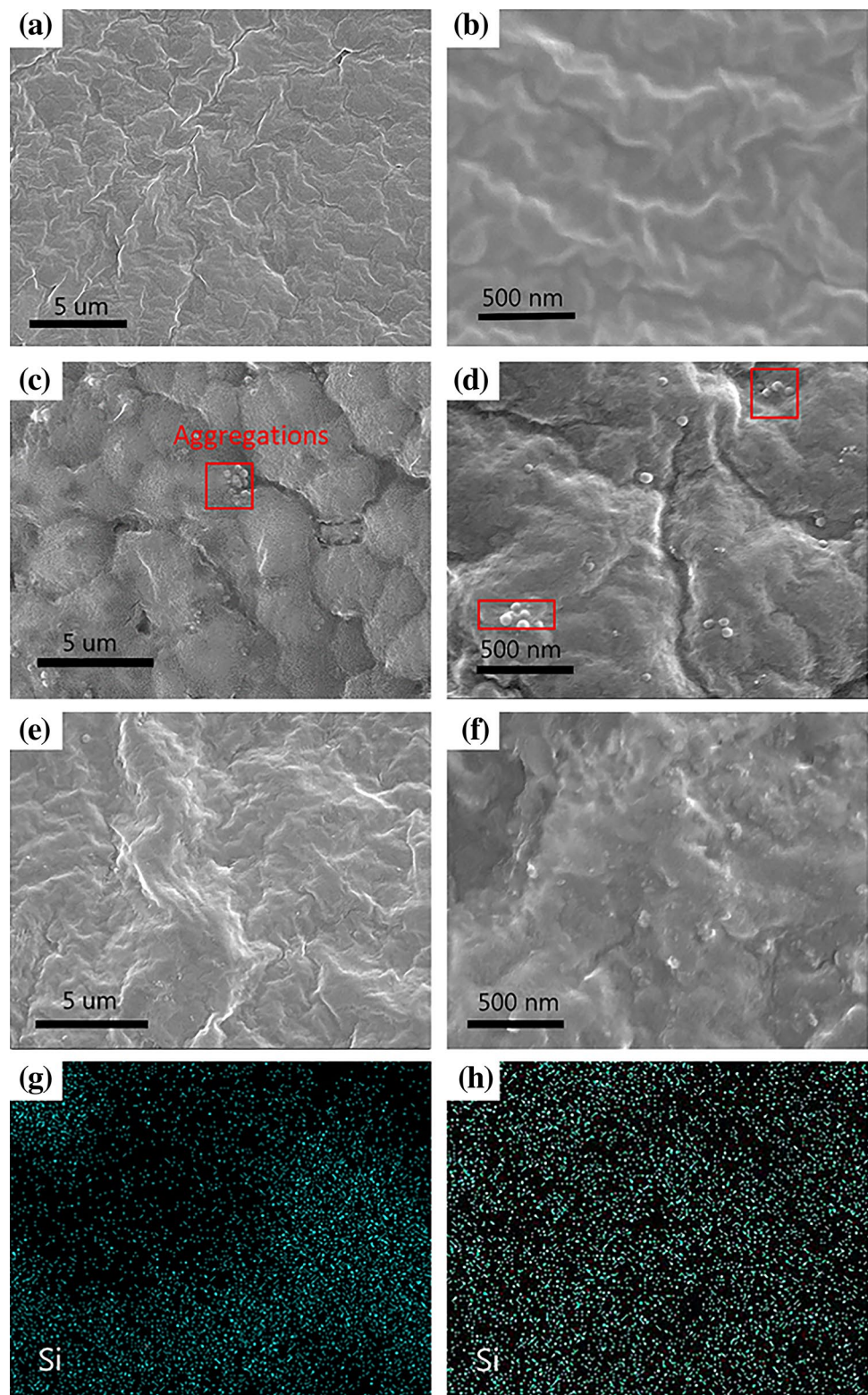
the SiO₂ nanoparticles, the surface of the microsphere is obviously rougher than before. TEM was used in order to further determine the morphology of the surface coating; it can be observed that the SiO₂ nanoparticles have clearly distinguishable coating layers and the thickness is estimated to be ~ 20 nm. Combined with the results of Fig. 1, we can fully conclude that SiO₂@PMMA nanoparticles have been successfully synthesized.

3.2 Physical properties of the composite polymer electrolyte

The surface of nano-SiO₂ usually contains a large number of –OH groups, and these –OH groups can act as a Lewis acid competing with lithium salt cations and provide more active

Li⁺ [38]. Although PMMA grafts onto SiO₂ nanoparticles, the surface still exists –OH groups, which can be confirmed by the broad peak around 3400 cm⁻¹ in Fig. 1a. In addition, the –OH group that partially remained on the surface of SiO₂ can promote the capture of impurities in electrolyte, and the existing ester group of PMMA can improve ionic conductivity and phase boundary stability. Therefore, the interfacial interaction between the polymer matrix and the inorganic particles can be enhanced. SEM was conducted on the composite electrolyte to investigate whether SiO₂@PMMA was uniformly dispersed. The SEM images of the composite electrolytes are shown in Fig. 3a–f. It can be found from Fig. 3a, b that the surface of the CPE is dense and smooth. Figure 3c, d is SEM images of CPE-SiO₂ prepared by mixing nano-SiO₂ into the polymer directly, in which we can

Fig. 3 SEM images of the **a** and **b** CPE, **c** and **d** CPE-SiO₂, and **e** and **f** CPE-(SiO₂@PMMA). **g** and **h** EDS mapping image of (c, e)



found distinct aggregation of nano-SiO₂ and inhomogeneous distribution. The surface morphology of the CPE-(SiO₂@PMMA) membrane presents a uniform morphology without any bare SiO₂ particles in Fig. 3c and f, indicating that

the SiO₂ particles are well dispersed and embedded in the polymer matrix. Besides, it can be found in Fig. 3 g, h that silicon (Si) element is mainly uniformly distributed on the surface of the CPE-(SiO₂@PMMA) membrane comparing

with CPE-SiO₂ membrane, confirming that the nanoparticles are well dispersed in the CPE-(SiO₂@PMMA) membrane.

High degree of crystallinity obstructs the movement of polymer chain segments and further hinders the transportation of lithium ions. Figure 4a depicts X-ray diffraction (XRD) patterns of nano-SiO₂ and three kinds of the CPE membranes. The XRD pattern for SiO₂ nanoparticles exhibited only a broadened peak around 26.64° with relatively weak intensity, demonstrating that the synthesized SiO₂ nanoparticles have an amorphous phase. However, the characteristic diffraction peak of the SiO₂ nanoparticles cannot be found in the prepared CPE film even in the CPE-SiO₂ film, which is mainly attributed to the Lewis acid–base interaction between the doped nanoparticles and the polymer matrix. It is also reported in other articles [31]. The sample of CPE shows broad diffraction peak at 15°–25° indicating CPE has a higher crystallinity. With the nanoparticles being doped

into the polymer matrix, the characteristic diffraction peaks of CPE-SiO₂ and CPE-(SiO₂@PMMA) become weaker and disappear gradually. As depicted in Fig. 4c, the diffraction intensity of CPE-(SiO₂@PMMA) is weakest because SiO₂@PMMA disrupts the crystallinity of the polymer. The results mentioned above indicate that the CPE-(SiO₂@PMMA) has the most amorphous regions to transport Li⁺. Consequently, we can speculate that CPE-(SiO₂@PMMA) membrane has the best electrochemical performance.

The thermal stability of the electrolyte is an important factor in determining the safety of the battery. Figure 4b demonstrates TG curves of three kinds of membranes. The decomposition temperature of the CPE-SiO₂ is about 330 °C, and the thermal decomposition temperature is significantly higher than that of the membrane without nano-SiO₂ doped, which is owing to the decent chemical inertness of the doped inorganic nanoparticles. The prepared

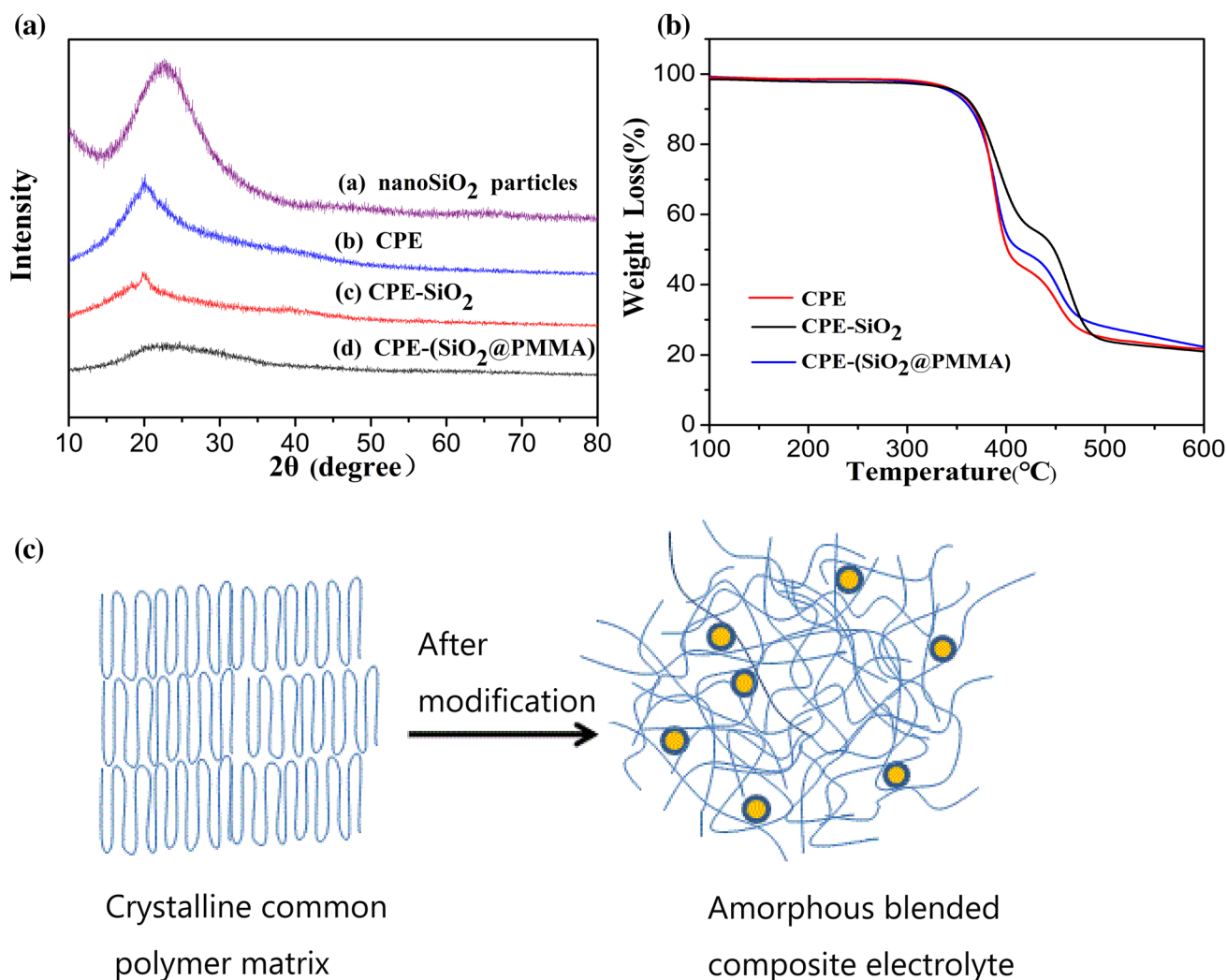


Fig. 4 XRD image **a** and TG curves **b** of CPE membrane, CPE-SiO₂ membrane, and CPE-(SiO₂@PMMA) membrane, **c** Illustration of nano-SiO₂@PMMA disrupting polymer crystallinity

SiO₂@PMMA hybrid particles contain the organic component MMA, which may cause the decomposition temperature of CPE-(SiO₂@PMMA) to be lower than CPE-SiO₂ at a certain temperature. This phenomenon has also been discussed in other articles [31, 40]. The above results indicate that the addition of suitable inorganic–organic hybrid particles can contribute to the thermal stability of the polymer matrix. Meanwhile, the decomposition temperature of the CPE-(SiO₂@PMMA) film up to 320 °C, which can completely meet the practical applications.

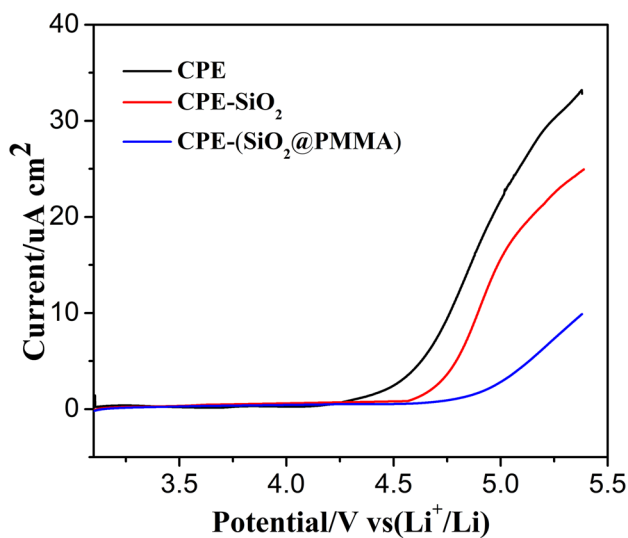


Fig. 5 LSV curves of the Li/CPEs/SS cells with the CPE, CPE-SiO₂, and CPE-SiO₂@PMMA membrane

3.3 Electrochemical stability and ionic conductivity

Plenty of high potential cathode materials have been developed in order to increase the energy density of batteries; however, most traditional electrolytes are difficult to match with these high voltage cathodes. The electrochemical working window of the assembled Li/CPEs/SS cells is investigated using LSV tests. As shown in Fig. 5, CPE, CPE-SiO₂ membrane decomposes at 4.3 V, 4.5 V, respectively, while CPE-(SiO₂@PMMA) membrane is stable until 4.7 V, which is higher than other composite electrolytes. This phenomenon can be attributed to two reasons. Firstly, the inorganic nanoparticles can interact with polymer matrix and TFSI⁻ anion to hold up their decomposition. Secondly, the uniformly dispersed SiO₂@PMMA nanoparticles have the functional sites for crosslinking with polymer segments which could stabilize the interface between the polymer and the inorganic filler.

Figure 6a illustrates the ionic conductivities of CPE-(SiO₂-PMMA) membranes from 20 to 80 °C, and shows the corresponding equivalent circuit. With temperature increasing, the conductivity exhibits an obvious increase, which attributed to the gradual polymer softening process and the increasing Li⁺ movement in the polymer network. It can be seen that the ionic conductivity is around 8.54 × 10⁻⁵ S cm⁻¹ at 60 °C, and the ionic conductivity further increases to 1.02 × 10⁻⁴ S cm⁻¹ at 80 °C. The ionic conductivity from 20 °C to 80 °C is displayed on an Arrhenius plot as shown in Fig. 6b; temperature dependence is non-linear and can be described by the Vogel–Tammán–Fulcher (VTF) model [41]. This non-linear behavior suggest that the polymer chains are driving ion solvation and transportation, and the transference of Li⁺ ions is a complex process involving ionic jumping between

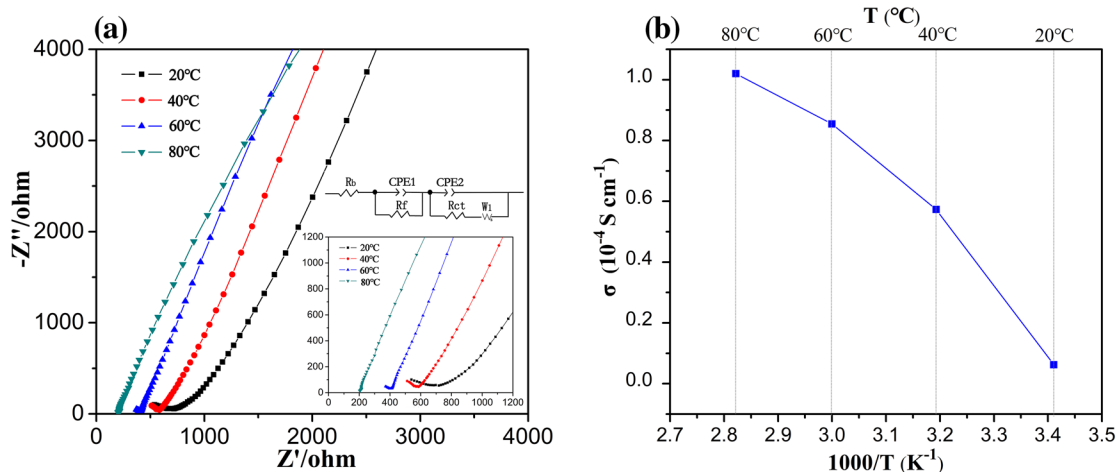


Fig. 6 a Impedance spectra of CPE-(SiO₂@PMMA) at different temperatures. b Dependency of the ionic conductivity of CPE-(SiO₂@PMMA) on the temperature

different sites of polymer chain, the segmental motion of polymeric chains, and so forth [38, 41]. In order to keep the mechanical strength of the composite polymer membrane, 60 °C was adopted as a measurement temperature in this study.

3.4 Interfacial stability against lithium metal electrode

The interface stability between lithium metal electrode and electrolyte is very significant for lithium metal batteries' application. As shown in Fig. 7 a, the interface resistances between CPE-(SiO₂@PMMA) and lithium metal remained stable during 15 days than those between CPE and CPE-SiO₂, suggesting an excellent compatibility with lithium electrode. With the storage time increasing, the interface impedance of the CPE changed quickly, while that of CPE-SiO₂ and CPE-(SiO₂@PMMA) continues to go up as well. However, when the SiO₂ and SiO₂@PMMA nanoparticles are doped into the polymer matrix, the interfacial resistance can achieve a relatively stable value quickly in 15-day storage which may be owing to the slow formation of the SEI film between the electrodes and CPE, CPE-(SiO₂@PMMA) electrolyte. The interfacial resistance of CPE-(SiO₂@PMMA) increases from 115 Ω on the first day to 1009 Ω after 15 days of storage, which is smaller than CPE-SiO₂, indicating that the uniform SiO₂@PMMA particles are helpful to form the low-impedance and steady SEI film on the surface of the electrodes to improve the cell performance. These results can be mainly attributed to the special size effect and excellent dispersibility of the added appropriate SiO₂@PMMA nanoparticles; on one hand, the Lewis acid character of the added SiO₂@PMMA nanoparticles would compete with the Lewis character of Li⁺ for the formation of complexes with the polymer chains, and on the other hand, SiO₂@PMMA nanoparticles can absorb impurities such as trace of organic solvent and water which could enhance the interfacial stability.

3.5 Cell performance

Applicability of the CPE in all solid battery was further evaluated by assembling a half-cell using Li_{0.8}Co_{0.1}Mn_{0.1}O₂ cathode and Li metal anode. As shown in Fig. 8a, the initial discharge capacity of cells with CPE, CPE-SiO₂, CPE-(SiO₂@PMMA) reach 140, 168, 182 mAh g⁻¹ at 0.5C, respectively. The capacity of the cell with CPE decreases fast to 61 mAh g⁻¹ after 76 cycles at 0.5 C and stop working; the reason is that the mechanical properties of the CPE are poor and the lithium dendrites may pierce the CPE membrane during cycling. The cells with CPE-(SiO₂@PMMA) exhibit excellent cycling performances, which remained above 81.7% capacity after 100 cycles at 0.5C, while the cell with CPE-SiO₂ exhibits a poor cycling performance comparing with CPE-(SiO₂@PMMA). These results may be caused by the unevenly distributed nano-SiO₂ and are consistent with the results of XRD.

Figure 8a–e compares the rate capability of LiNi_{0.8}Co_{0.1}Mn_{0.1}O₂|Li cell with three types of electrolyte at various discharge rates. The cell with CPE-(SiO₂@PMMA) exhibits a good rate performance; even at a discharge rate of 5 C, the discharge capacity remained at 105 mAh g⁻¹, and when the discharge rate was switches to 0.2 C, the discharge capacity could recover to the primary value, which is much better than the rate performance of the cells with CPE-SiO₂ and CPE as shown in Fig. 8b–f. The reasons for these outstanding cyclic performance and rate capability are threefold. First, the improvement of cell performance is ascribed to the Lewis acid–base interaction between SiO₂@PMMA and the polymer matrix. SiO₂@PMMA acts as a Lewis acid–base reaction center and forms a lot of temporary O/Li⁺ or OH/[TFSI]⁻ sites on the surface [42]. The transient formation–destruction of these temporary bonds not only promotes the dissociation of Li salt, but also provides additional sites for transporting Li⁺ in the CPE, providing more freely migrating Li⁺ [35, 40]. Second, the strong interaction between SiO₂@PMMA and the polymer chain can effectively lock the polymer chain, modify the

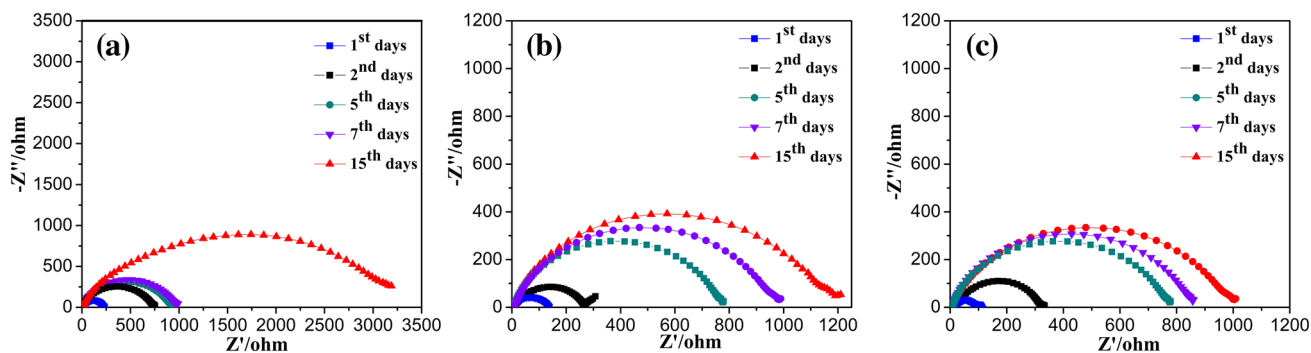


Fig. 7 Impedance spectra for the assembled Li/CPEs/Li cells for various storage times at 60 °C (a CPE; b CPE-SiO₂; c CPE-SiO₂@PMMA)

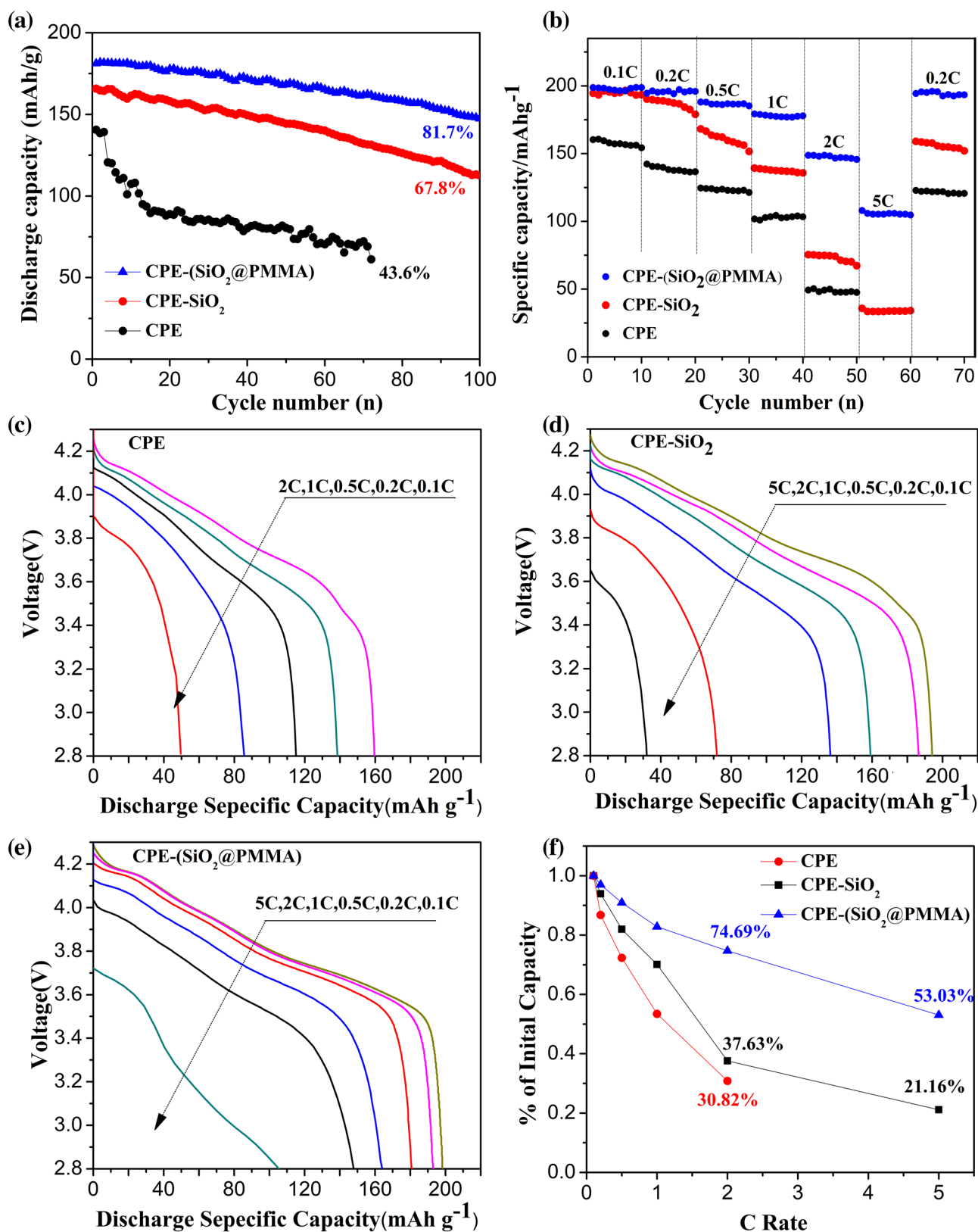


Fig. 8 **a** Cycling performances of CPE, CPE-SiO₂, CPE-SiO₂@PMMA at 0.5 C discharge rate. **b** Rate performance of CPE, CPE-SiO₂, CPE-SiO₂@PMMA at different current densities. **c–e** Discharge curves of the synthesized CPE, CPE-SiO₂, CPE-SiO₂@

PMMA samples, respectively, on cycling sequentially from 0.1 to 5 C. **f** Evolution of normalized capacity as a function of discharge rate for three different composite membranes

polymer conformation, prevent polymer chain recombination, and maintain the low crystallinity state of the polymer matrix. Finally, PMMA-coated SiO₂ can contribute a homogeneous distribution of SiO₂ in composite electrolyte, avoiding the agglomeration of fillers, which provides a high ionic conductivity and improves interfacial stability. All these results proved that the CPE-(SiO₂@PMMA) is a promising solid electrolyte for Li metal batteries to build a high-energy system.

4 Conclusion

In conclusion, a high-performance composite polymer electrolyte with SiO₂@PMMA hybrid nanoparticles is demonstrated in this research. SiO₂@PMMA nanoparticles enhance the compatibility of nanoparticles with polymer matrix and promote migration of active Li⁺, and thus the CPE-(SiO₂@PMMA) electrolyte performs lower crystallinity, a high ionic conductivity, and excellent interfacial stability. The performance of LiNi_{0.8}Co_{0.1}Mn_{0.1}O₂/CPE/Li half-cell with CPE-(SiO₂@PMMA) electrolyte is greatly enhanced compared to those with other electrolytes. Its initial capacity is maintained at 148.6 mAh g⁻¹ and capacity retention is 81.7% after 100 cycles at 0.5 C, whereas the cell with CPE membrane was broken with 100 cycles unfinished. Even at high rate discharge condition (5 C), the specific capacity is 108.4 mAh g⁻¹, which was better than that of the CPE cell being 34.5 mAh g⁻¹. This work suggests that blended P(VDF-HFP)/PEO/PMMA-based polymer membrane doped with 4 wt% PMMA-coated SiO₂ hybrid nanoparticles is a promising polymer electrolyte for the flexible lithium metal battery.

References

1. M. Armand, J.M. Tarascon, Building better batteries. *Nature* **451**(7179), 652–657 (2008)
2. J.B. Goodenough, Energy storage materials: a perspective. *Energy Storage Mater.* **1**, 158–161 (2015)
3. J.B. Goodenough, Y. Kim, Challenges for rechargeable Li batteries. *Chem. Mater.* **22**, 587–603 (2010)
4. W.K. Shin, J. Cho, A.G. Kannan et al., Cross-linked composite gel polymer electrolyte using mesoporous methacrylate-functionalized SiO₂ nanoparticles for lithium-ion polymer batteries. *Sci. Rep.* **6**, 26332 (2016)
5. P. Wang, J. Chai, Z. Zhang et al., An intricately designed poly(vinylene carbonate-acrylonitrile) copolymer electrolyte enables 5 V lithium batteries. *J. Mater. Chem. A* **7**, 5295–5304 (2019)
6. A. Mauger, M. Armand, C.M. Julien et al., Challenges and issues facing lithium metal for solid-state rechargeable batteries. *J. Power Sources* **353**, 333–342 (2017)
7. Q. Wang, H. Zhang, Z. Cui et al., Siloxane-based polymer electrolytes for solid-state lithium batteries. *Energy Storage Mater.* **23**, 466–490 (2019)
8. L. Fan, S. Wei, S. Li et al., Recent progress of the solid-state electrolytes for high-energy metal-based batteries. *Adv. Energy Mater.* **8**(11), 1702657 (2018)
9. J.G. Kim, B. Son, S. Mukherjee et al., A review of lithium and non-lithium based solid state batteries. *J. Power Sources* **282**, 299–322 (2015)
10. D. Li, L. Chen, T. Wang et al., 3D fiber-network-reinforced bicontinuous composite solid electrolyte for dendrite-free lithium metal batteries. *ACS Appl. Mater. Interfaces* **10**(8), 7069–7078 (2018)
11. M. Faridi, L. Naji, S. Kazemifard et al., Electrochemical investigation of gel polymer electrolytes based on poly(methyl methacrylate) and dimethylacetamide for application in Li-ion batteries. *Chem. Papers* **72**, 2289–2300 (2018)
12. T. Ma, Z. Cui, Y. Wu et al., Preparation of PVDF based blend microporous membranes for lithium ion batteries by thermally induced phase separation: I—Effect of PMMA on the membrane formation process and the properties. *J. Membr. Sci.* **444**(10), 213–222 (2013)
13. H.P. Zhang, P. Zhang, Z.H. Li et al., A novel sandwiched membrane as polymer electrolyte for lithium ion battery. *Electrochem. Commun.* **9**(7), 1700–1703 (2007)
14. H. Zhang, J. Zhang, J. Ma et al., Polymer electrolytes for high energy density ternary cathode material-based lithium batteries. *Electrochem. Energy Rev.* **2**, 128–148 (2019)
15. J.I. Kim, Y. Choi, K.Y. Chung et al., A structurable gel-polymer electrolyte for sodium ion batteries. *Adv. Funct. Mater.* **27**, 1701768 (2017)
16. C.H. Tsao, P.L. Kuo, Poly(dimethylsiloxane) hybrid gel polymer electrolytes of a porous structure for lithium ion battery. *J. Membr. Sci.* **489**, 36–42 (2015)
17. N.H. Idris, M.M. Rahman, J.Z. Wang et al., Microporous gel polymer electrolytes for lithium rechargeable battery application. *J. Power Sources* **201**, 294–300 (2012)
18. Q. Xiao, X. Wang, W. Li et al., Macroporous polymer electrolytes based on PVDF/PEO-b-PMMA block copolymer blends for rechargeable lithium ion battery. *J. Membr. Sci.* **334**(1–2), 117–122 (2009)
19. M.M. Rao, J.S. Liu, W.S. Li et al., Performance improvement of poly(acrylonitrile-vinyl acetate) by activation of poly(methyl methacrylate). *J. Power Sources* **189**(1), 711–715 (2009)
20. Y.H. Liao, X.P. Li, C.H. Fu et al., Performance improvement of polyethylene-supported poly(methyl methacrylate-vinyl acetate)-co-poly(ethylene glycol) diacrylate based gel polymer electrolyte by doping nano-Al₂O₃. *J. Power Sources* **196**(16), 6723–6728 (2011)
21. S.J. Tan, X.X. Zeng, Q. Ma et al., Recent advancements in polymer-based composite electrolytes for rechargeable lithium batteries. *Electrochem. Energy Rev.* **1**(2), 113–138 (2018)
22. T. Sakakibara, M. Kitamura, T. Honma et al., Cross-linked polymer electrolyte and its application to lithium polymer battery. *Electrochim. Acta* **296**, 1018–1026 (2019)
23. H. Huang, D. Fei, Z. Hai et al., Nano-SiO₂ embedded poly(propylene carbonate)-based composite gel polymer electrolyte for lithium-sulfur batteries. *J. Mater. Chem. A* **6**, 9539–9549 (2018)
24. S. Liu, N. Imanishi, T. Zhang, A. Hirano, Y. Takeda, O. Yamamoto, J. Yang, Effect of nano-silica filler in polymer electrolyte on Li dendrite formation in Li/poly(ethyleneoxide)-Li(CF₃SO₂)₂N/Li. *J. Power Sources* **195**, 6847–6853 (2010)
25. X. He, Q. Shi, X. Zhou et al., In situ composite of nano SiO₂-P(VDF-HFP) porous polymer electrolytes for Li-ion batteries. *Electrochim. Acta* **51**(6), 1069–1075 (2005)
26. N. Wu, Q. Cao, X. Wang et al., In situ ceramic fillers of electrospun thermoplastic polyurethane/poly(vinylidene fluoride) based gel polymer electrolytes for Li-ion batteries. *J. Power Sources* **196**(22), 9751–9756 (2011)

27. J.W. Zha, N. Huang, K.Q. He et al., Electrospun poly(ethylene oxide) nanofibrous composites with enhanced ionic conductivity as flexible solid polymer electrolytes. *High Volt.* **2**(1), 25–31 (2017)
28. Z.H. Li, H.P. Zhang, P. Zhang et al., Effects of the porous structure on conductivity of nanocomposite polymer electrolyte for lithium ion batteries. *J. Membr. Sci.* **322**(2), 416–422 (2008)
29. Y. Chen, H. Chen, F. Lin et al., Preparation and conductivity of the composite polymer electrolytes based on poly[bis(methoxyethoxyethoxy)-phosphazene], LiClO₄ and α -Al₂O₃. *Solid State Ion.* **156**(3), 383–392 (2003)
30. K.M. Kim, J.M. Ko, N.G. Park et al., Characterization of poly(vinylidene fluoride-co-hexafluoropropylene)-based polymer electrolyte filled with rutile TiO₂ nanoparticles. *Solid State Ion. Diffus. React.* **161**(1–2), 121–131 (2003)
31. Z. Wang, C. Miao, W. Xiao et al., Effect of different contents of organic-inorganic hybrid particles poly(methyl methacrylate) ZrO₂ on the properties of poly(vinylidene fluoride-hexafluoropropylene)-based composite gel polymer electrolytes. *Electrochim. Acta* **272**, 127–134 (2018)
32. J. Cao, L. Wang, X. He et al., In situ prepared nano-crystalline TiO₂-poly(methyl methacrylate) hybrid enhanced composite polymer electrolyte for Li-ion batteries. *J. Mater. Chem. A* **1**(19), 5955 (2013)
33. X. Zuo, J. Wu, X. Ma et al., A poly(vinylidene fluoride)/ethyl cellulose and amino-functionalized nanoSiO₂ composite coated separator for 5 V high-voltage lithium-ion batteries with enhanced performance. *J. Power Sources* **407**, 44–52 (2018)
34. L.P. Wang, T.S. Wang, Y.X. Yin et al., Exploiting lithium-depleted cathode materials for solid-state li metal batteries. *Adv. Energy Mater.* **9**, 1901335 (2019)
35. G.H. Bogush, M.A. Tracy, C.F.Z. Iv, Preparation of monodisperse silica particles: control of size and mass fraction. *J. Non-Cryst. Solids* **104**(1), 95–106 (1988)
36. W. Liu, W. Li, D. Zhuo et al., Core-shell nanoparticle coating as an interfacial layer for dendrite-free lithium metal anodes. *ACS Central Sci.* **3**(2), 135 (2017)
37. Y. Hu, T. Zhang, J. Ge et al., Superparamagnetic composite colloids with anisotropic structures. *J. Am. Chem. Soc.* **129**(29), 8974–8975 (2007)
38. Y. Zhu, J. Cao, H. Chen et al., High electrochemical stability of a 3D cross-linked network PEO@nano-SiO₂ composite polymer electrolyte for lithium metal batteries. *J. Mater. Chem. A* **7**, 6832–6839 (2019)
39. C. Ton-That, A.G. Shard, D.O.H. Teare et al., XPS and AFM surface studies of solvent-cast PS/PMMA blends. *Polymer* **42**(3), 1121–1129 (2001)
40. D. Lin, W. Liu, Y. Liu et al., High ionic conductivity of composite solid polymer electrolyte via in situ synthesis of monodispersed SiO₂ nanospheres in poly(ethylene oxide). *Nano Lett.* **16**(1), 459–465 (2016)
41. L. Long, S. Wang, M. Xiao et al., Polymer electrolytes for lithium polymer batteries. *J. Mater. Chem. A* **4**, 10038–10069 (2016)
42. H. Huang, F. Ding, H. Zhong et al., Nano-SiO₂ embedded poly(propylene carbonate)-based composite gel polymer electrolyte for lithium-sulfur batteries. *J. Mater. Chem. A* **10**(6), 9539–9549 (2018)

Publisher's Note Springer Nature remains neutral with regard to jurisdictional claims in published maps and institutional affiliations.